ACS APPLIED MATERIALS & INTERFACES

Research Article

www.acsami.org

DNA-Base Guanine as Hydrogen Getter and Charge-Trapping Layer Embedded in Oxide Dielectrics for Inorganic and Organic Field-Effect Transistors

Junyeong Lee,[†] Ji Hoon Park,[†] Young Tack Lee,[†] Pyo Jin Jeon,[†] Hee Sung Lee,[†] Seung Hee Nam,[†,‡] Yeonjin Yi,[†] Younjoo Lee,[†] and Seongil Im*[,†]

[†]Institute of Physics and Applied Physics, Yonsei University, 262 Seongsanno, Seodaemun-gu, Seoul 120-749, Korea

[‡]R&D Center, LG Display, Paju 413-811, Korea

Supporting Information

ABSTRACT: DNA-base small molecules of guanine, cytosine, adenine, and thymine construct the DNA double helix structure with hydrogen bonding, and they possess such a variety of intrinsic benefits as natural plentitude, biodegradability, biofunctionality, low cost, and low toxicity. On the basis of these advantages, here, we report on unprecedented useful applications of guanine layer as hydrogen getter and charge trapping layer when it is embedded into a dielectric oxide of n-channel inorganic InGaZnO and p-channel organic heptazole field effect transistors (FETs). The embedded guanine layer much improved the gate stability of inorganic FETs gettering many hydrogen atoms in the gate dielectric layer of FET, and it also played as charge trapping layer to which the voltage pulse-driven charges might be injected from channel, resulting in a threshold voltage (V_{th}) shift of FETs. Such shift state is very ambient-stable and almost irrevocable even under a high electric-field at room temperature. So, Boolean logics are nicely demonstrated by using our FETs with the guanine-embedded dielectric. The original V_{th} is recovered only under high energy blue photons by opposite voltage pulse (charge-ejection), which indicates that our device is also applicable to nonvolatile photo memory.

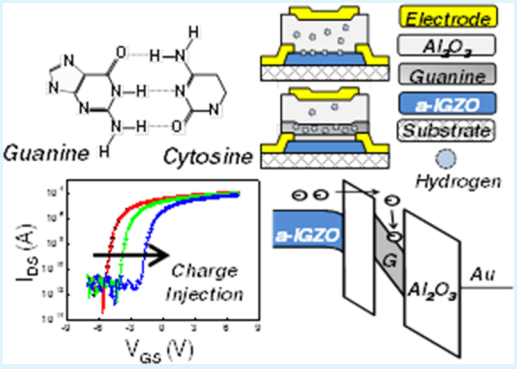

KEYWORDS: *DNA-base molecule, guanine, electrical stability, field-effect transistor, logic inverter*

INTRODUCTION

Polymer chain deoxyribonucleic acid (DNA) researches have been mainly oriented to biomedical or biochemical applications. Following the bioresearch, DNA has recently been studied as one of the interesting candidates for future electronic materials, too, because it has such a variety of intrinsic benefits as its natural plentitude, biodegradability, biofunctionality, low cost, and low toxicity.[1−5] For example, light emission efficiency in organic light-emitting diode (OLED) was highly improved when DNA polymer was used as an electron blocking layer.[6,7] Also, DNA polymer was used as a dielectric layer for field-effect transistors (FETs), although its dielectric behavior turned out to be unstable.[8−12] However, because of the insolubility of DNA polymer in typical organic solvent, additional purifying process with a cationic surfactant complex should be accomplished for optoelectronic or electronic application. On the one hand, DNA-base small molecules such as guanine, cytosine, adenine, and thymine, which construct the DNA double helix structure with hydrogen bonding, are able to form a deposited thin film by thermal evaporation and readily patterned by conventional method.[13−15] Such DNA-base small molecule layers are electrically insulating and were adopted for a dielectric for organic FETs, although their dielectric stability again remains questionable if they aren't leaning on an adjacent inorganic insulating layer.

Here, we report on unprecedented useful applications of DNA-base small molecule guanine ($C_5H_5N_5O$) layer as hydrogen getter and charge trapping layer when it is embedded into a dielectric oxide of inorganic and organic FETs. Because thermal evaporation-deposited guanine layer plays as H getter during low temperature (100 °C) process of atomic layer deposited (ALD) dielectric oxide, the dielectric becomes more electrically stable than the case without the DNA-base guanine layer, and moreover the embedded guanine plays as a trap layer for injected charges from the channel of the FET, so that the voltage pulse-driven charge injection simply leads to the threshold voltage (V_{th}) shift of the inorganic FET.[16−19] Because such a V_{th} shift is very ambient-stable and is almost irrevocable even under a high electric (E)-field at a room temperature, Boolean logics are nicely demonstrated by using our FETs with the DNA base-embedded dielectric. Such a V_{th} shift by guanine trap layer is demonstrated for both n-channel InGaZnO

Received: December 27, 2013
Accepted: February 10, 2014
Published: February 10, 2014

   dx.doi.org/10.1021/am405998d | *ACS Appl. Mater. Interfaces* 2014, 6, 4965−4973

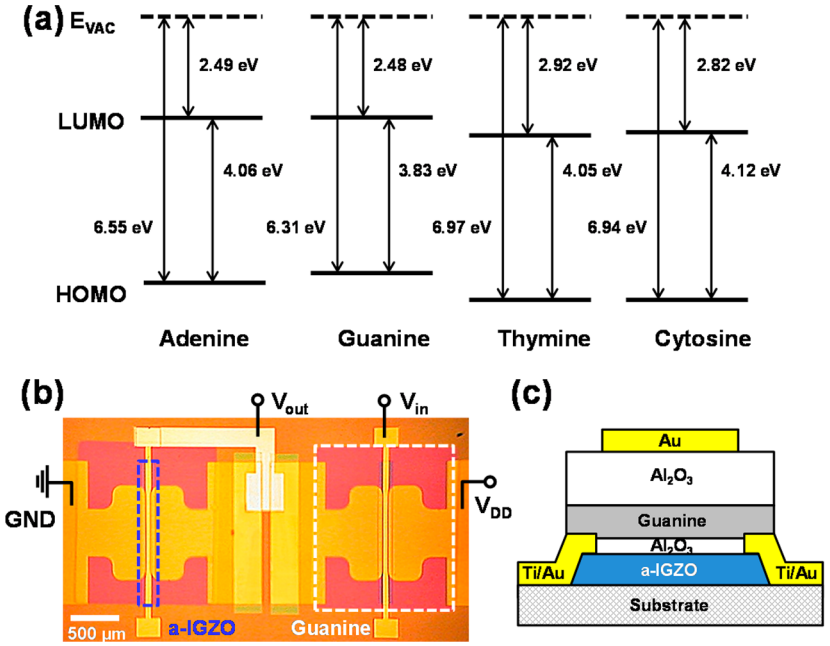

Figure 1. (a) Schematic energy-level diagrams of DNA-base materials including adenine, guanine, thymine and cytosine thin films with vacuum-level (E_{vac}) alignment. The HOMO-LUMO gaps, electron affinities, and ionization energies were determined by ultraviolet photoemission spectroscopy (UPS) measurement. (b) Optical microscopy image of the top-view of our inverter comprised of two a-IGZO FETs which were connected in series. The a-IGZO channel and embedded guanine layer are indicated by blue and white dashed lines. (c) Schematic cross-section image of the a-IGZO FET with embedded guanine getter/charge trapping layer.

(IGZO) and p-channel organic heptazole FETs, and the original V_{th} is only obtained by blue photons with ~2.7 eV, whereas lower energy photons do not work.

EXPERIMENTAL METHODS

Fabrication of IGZO FETs with Guanine-Embedded Dielectric. On a precleaned corning glass substrate with a 350 nm SiO_2 grown by plasma-enhanced chemical vapor deposition system (PECVD), we deposited a 50 nm thick amorphous-InGaZnO (a-IGZO) thin film through DC magnetron sputtering system at room temperature. Patterning process was done by conventional photolithography and wet etching process using diluted buffered oxide etchant (B.O.E) solution (200:1) and then a-IGZO was annealed at 200 °C for 2 h in ambient using hot-plate. The source and drain electrodes of Ti/Au (50 nm/50 nm) bilayer were deposited by DC magnetron sputtering system and patterned by photolithography and lift-off process. The lift-off technique was achieved by the lift-off-layer (LOL 2000: Micro Chem) and photo-resist layer (SPR 3612: Micro Chem). The defined-channel width/length ratio was 1000 μm/50 μm. After that, atomic layer deposition (ALD) system was used for aluminum-oxide (Al_2O_3) as tunneling (5 nm) and blocking (40 nm) layers, while 20 nm-thin DNA-base material (here, guanine) was inserted between them. DNA-base thin films are carefully deposited by thermal evaporation system (at 200 °C for the guanine, 95 °C for the cytosine, 85 °C for the adenine, 80 °C for the thymine), to play as a charge trapping layer between them. ALD process was maintained at a temperature lower than 100 °C in consideration of the thermal limit of guanine layer in vacuum (~0.5 Torr). The Al_2O_3 etching for source-drain contact definition was performed with the same dilute B.O.E as used in the IGZO patterning. Finally, opaque gold (Au) or transparent indium–tin-oxide (ITO) thin-film was deposited for the gate electrode of a-IGZO thin-film transistors (TFTs). (Schematic device cross section is described in Figure 1c). Logic inverter and Boolean logic devices were then fabricated by interconnecting Al as shown in Figure 1b.

Fabrication of Heptazole FETs with Guanine-Embedded Dielectric. The bottom gate and top contact organic FET with heptazole semiconductor channel was also fabricated on a precleaned corning glass substrate. Bottom Al gate electrode was thermally evaporated through a shadow mask for patterning at first. Then 40 nm thick and 5 nm thin Al_2O_3 layer were grown by the ALD process, whereas a guanine layer (20 nm) was inserted in between those two Al_2O_3 layers by thermal evaporation system. Here, deposition sequence for our guanine embedded dielectric was opposite to IGZO FETs. Then 60 nm-thin heptazole channel layer (width/length = 500/90 μm) was patterned on the thin charge tunneling Al_2O_3 layer by organic molecule beam deposition (OMBD) system as we purchased the heptazole small-molecule from our co-workers (Luminano Co). Finally, gold electrode was employed for ohmic source and drain contact.

Electrical and Photoelectric Measurements. The device current–voltage (I–V) characterizations were carried out by a semiconductor parameter analyzer (HP 4155C, Agilent Technologies). Electrical dynamics measurements were investigated with a function generator (AFG 310, Sony/Tektronix) and an oscilloscope (TDS210, Tektronix). Photoelectric measurements were also implemented on both of our a-IGZO and Heptazole FETs with guanine-embedded dielectric by using light-emitting diodes (LEDs) with three different energies (wavelengths): red (680 nm), green (540 nm), and blue (440 nm). The optical power of the LEDs was given as 4, 2, and 1.5 mW for red, green, and blue in the same distance from the target FET.

Ultraviolet and X-ray Photoelectron Spectroscopy (UPS and XPS). The UPS and XPS were carried out in an ultrahigh vacuum multi-chamber system composed of analysis and preparation chambers which were maintained at a pressure of 3×10^{-9} and 2×10^{-8} Torr, respectively. For UPS analysis, we prepared four types of DNA base thin-films on ITO substrate. After deposition of DNA-base films by thermal evaporation system, the sample was transferred into the UPS chamber within 5 minutes. The UPS spectra were obtained with a sample bias of −15 V in normal emission geometry to measure the secondary electron cut-off. For XPS analysis, we deposited 3 nm thin guanine layer by thermal evaporation on a highly doped silicon substrate (p^{++} Si). After that, the substrates with and without thin guanine layer were put into ALD chamber for 3 nm-thin Al_2O_3 layer deposition on both samples, so that Al_2O_3 on p^{++} Si and Al_2O_3/guanine on p^{++} Si samples were achieved.

dx.doi.org/10.1021/am405998d | ACS Appl. Mater. Interfaces 2014, 6, 4965–4973

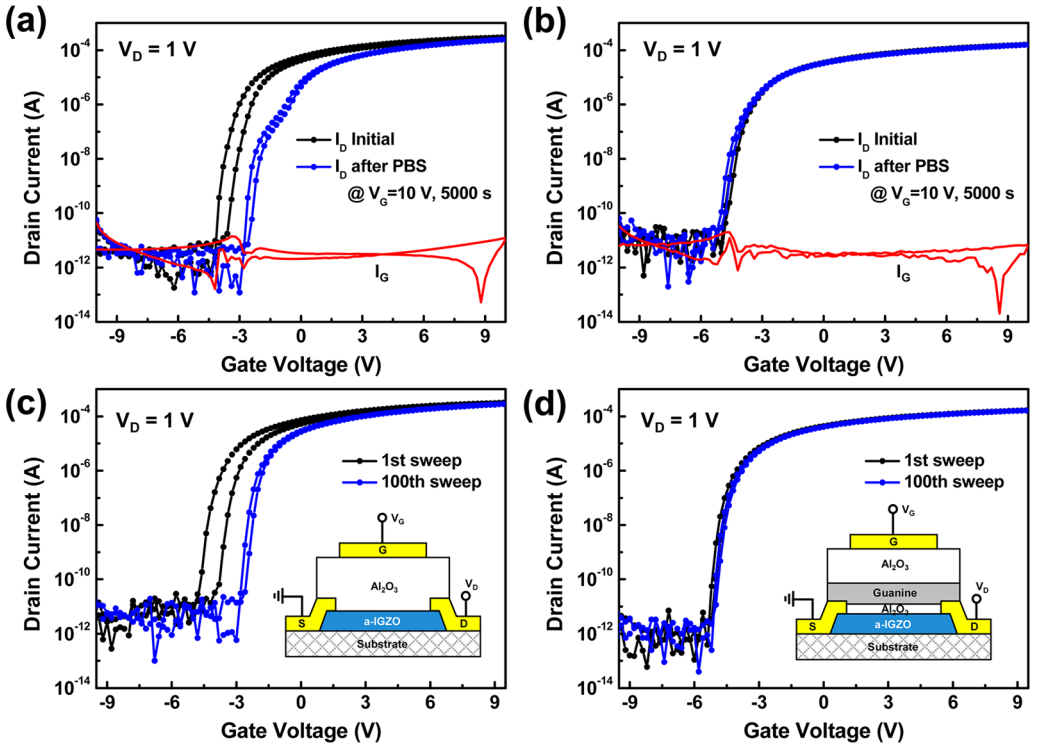

Figure 2. Transfer characteristics of a-IGZO FETs before and after positive gate bias stress (PBS). PBS tests were performed under the condition V_G = 10 V, V_D = 1 V, 5000 s for the both FETs (a) without and (b) with guanine layer. Transfer characteristics for devices (c) without and (d) with guanine layer as tested at V_D = 1 V under multiple gate voltage sweep up to 100 times.

Optical Absorption. The 20 nm thin DNA-base films of adenine, guanine, cytosine, and thymine were deposited on glass and taken to optical absorption measurement system, to measure their respective highest occupied molecular orbital-lowest unoccupied molecular orbitals (HOMO-LUMO) gaps.

Film Thickness, X-ray Diffraction, and Surface Morphology. The film thickness of guanine, other DNA-base films, and tunneling/blocking Al_2O_3 films was measured by using a mechanical profiler (alpha-step) and optical ellipsometry method. Crystalline quality and surface morphology of thick 150 nm thick guanine was characterized by Cu−Kα X-ray diffraction (XRD) and atomic force microscopy (AFM) after the film was deposited on a Si wafer. Details of AFM and XRD results are shown in Figures S1a, b in the Supporting Information, respectively.

RESULTS AND DISCUSSION

A. Device Structure of a-IGZO FETs with Embedded Guanine Molecule Layer. Figure 1a shows the energy diagrams including the highest occupied molecular orbital-lowest unoccupied molecular orbitals (HOMO-LUMO) gaps, electron affinities, and ionization energies, which were obtained from adenine, guanine, thymine, and cytosine thin films by ultraviolet photoemission spectroscopy (UPS) and optical absorption measurements (Figure S2 in the Supporting Information shows the absorption spectra of 20 nm thin DNA-base molecule layers).[20] Among the four molecules, guanine solely survived the present atomic layer deposition (ALD) process for Al_2O_3 dielectric formation which was conducted at 100 °C, whereas other DNA small molecule thin films could not endure the consecutive ALD process (for blocking Al_2O_3 layer) following DNA-base layer deposition. It is because the guanine−guanine pair is the most stably stacked in comparison with those of three other kinds of molecules, and because the highest melting point of 360 °C and high density of 2.2 g/cm^3 in guanine could probably prevent any decomposition of the molecule layer.[21,22] In the present study, we thus focused on the electronic properties of guanine thin film (3.83 and 2.48 eV as HOMO−LUMO gap and electron affinity, respectively), and chose the guanine layer to be embedded between ALD oxides for our logic and memory device design. The device cross section of an top-contact top-gate structured amorphous-InGaZnO (a-IGZO) FET of Figure 1c now shows 5 nm thin Al_2O_3, 20 nm-thin guanine, and 40 nm thin Al_2O_3, respectively stacked as tunneling, charge trapping, and blocking layers.[23,24] The top view of a-IGZO FET is displayed as an optical microscopy image in Figure 1b, where two FETs are connected in series each other as a driver (right) and a load (left) to form an inverter structure. Channel width/length (W/L) ratio was 1000 μm/50 μm. White and blue dashed lines indicate our embedded guanine and IGZO channel areas, respectively (more details of process steps are introduced in the Experimental Section).

B. Guanine Layer as H Atom Getter in a-IGZO FETs. Our a-IGZO FET with embedded guanine layer appeared very electrically stable under a positive gate bias stress (PBS), compared to the other FET without guanine layer as shown in panels a and b in Figure 2. According to the drain current-gate voltage (I_D−V_G) transfer curve of Figure 2a, the IGZO FET without DNA-base layer in Al_2O_3 dielectric does show significant threshold voltage shift (ΔV_{th}) toward positive voltage direction along with a hump due to the PBS (condition: V_G = 10 V, drain voltage V_D = 1 V for 5000 s), whereas it also reveals a hysteresis in its initial sweep. The threshold voltage shift and initial hysteresis were estimated as 2.27 V and 0.60 V, respectively. In contrast, our FET device with DNA-base guanine layer hardly displays such bias-stress-induced ΔV_{th} and gate hysteresis. More about the gate hysteresis behavior of less

dx.doi.org/10.1021/am405998d | ACS Appl. Mater. Interfaces 2014, 6, 4965−4973

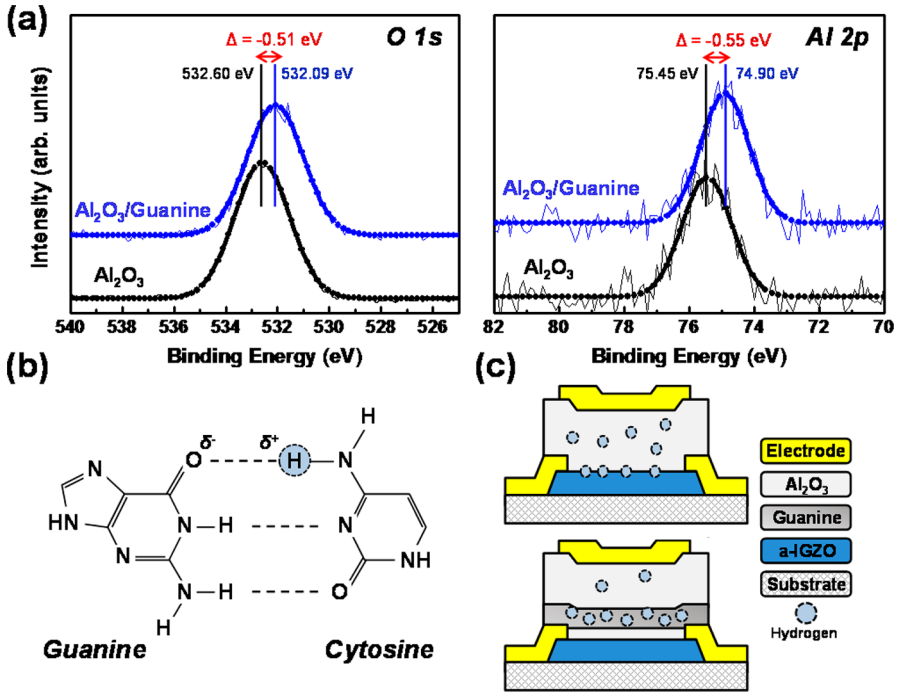

Figure 3. (a) XPS spectra of Al_2O_3/guanine and Al_2O_3 layer on highly doped silicon substrate. To determine the role of guanine during ALD oxide growth, we examined electron binding energies of oxygen 1s and aluminum 2p orbital. (b) Schematic molecular structure of three hydrogen bonds between the guanine ($C_5H_5N_5O$) and cytosine ($C_4H_5N_3O$) pair. Dashed lines indicate hydrogen bonds (δ^-–δ^+) between guanine and cytosine molecule, whereas blue circle does H atoms in the bond. (c) Schematic device cross-sections after ALD-growth of Al_2O_3 blocking layer for both cases, without and with guanine. H atoms that are the defect source may stay in guanine, not reaching to the 5 nm thin Al_2O_3 or Al_2O_3/a-IGZO interface as gettered by guanine itself.

stable device is addressed in panels c and d in Figure 2 (more details are in Figure S3 in the Supporting Information). These transfer curves with 100 times of continuous sweep also show the poor device stability of the IGZO FETs without guanine layer in terms of ΔV_{th} (= 1.70 V) and initial hysteresis (= 0.75 V). The measured value of C_{ox} is 75.0 nF/cm^2 for our guanine embedded dielectric, and dielectric constant of guanine is calculated to be ~5.02 whose value seems slightly higer than reference.[13] The linear mobility of our devices after 5000 s PBS was estimated at Figure S4 in the Supporting Information to be ~8.8 and ~8.3 cm^2/V s for the device without and with guanine layer embedded, respectively.

The device stabilities certainly come from the gate dielectric with the embedded DNA-base layer, but require an appropriate explanation, which is related to the DNA-base molecules themselves. To find out the proper reason, we carried out X-ray photoelectron spectroscopy (XPS) measurements with two cases on highly doped silicon substrate: one is Al_2O_3/guanine layer, and the other is only Al_2O_3 layer. To prevent the charging problem, we controlled each layer thickness to be only 3 nm. The XPS spectra in Figure 3a show the electron binding energy of oxygen 1s (O 1s) orbital and aluminum 2p (Al 2p) orbital. The binding energies of the case with guanine layer show smaller values for both O 1s (as 0.51 eV) and Al 2p (as 0.55 eV) than those of the case without guanine. These differences are attributed to the hydrogen atoms, which are supposed to stay in the low temperature Al_2O_3 but now some of them are rather incorporated into guanine during ALD deposition. According to the literature,[25,26] ALD-grown Al_2O_3 is supposed to have lower binding energies for both O 1s and Al 2p XPS signals as the oxide loses H atoms in its inside (see Table S1 in the Supporting Information for more details). The molecular structure of a single guanine (G) molecule ($C_5H_5N_5O$) is described in Figure 3b, where some of H and O bridging atoms of guanine need to be paired with other atoms of cytosine (C) molecule (G–C dipole pair: δ^-–δ^+). In the present situation, our G molecules have no pairing cytosine molecules, but instead expect many H and O atoms from Al_2O_3 ALD process (involved with precursor, reactant, and biproduct),[27,28] so that G molecules may easily take those atoms to fit in the hydrogen bonds that replace the dipole pairing. In addition, H atoms usually deliver a positive charge and G molecules may then take H^+ ions because guanine is a base material in its chemical nature. (An acid material is supposed to give H^+ ions). In this case, guanine tends to have direct chemical bonds with H ions instead of dipole interaction, so it is possible for guanine molecules to capture H ions according to literatures.[29,30] H atoms in the oxide dielectric diffuse into the IGZO/Al_2O_3 interface,[31] resultantly to cause high density interface traps (linked to several types of oxygen vacancies in IGZO) which are the source of the device instability.[32−35] Now, if the G molecules in the embedded layer getter those H atoms or H ions, the gate dielectric stability is successfully achieved by blocking the ALD-induced H atoms from coming down to the IGZO/Al_2O_3 interface. The device scheme of Figure 3c further illustrates the H blocking effects by G molecule layer, comparing the two cases with and without G layer. We believe that the G molecule layer may play a role as a getter for H atoms.

C. Guanine Layer As Charge Trapping Medium. Because the guanine molecule layer is now located above the 5 nm-thin Al_2O_3 tunneling layer as illustrated in Figure 1c, electron charges can be injected from IGZO channel to the guanine layer by a positive voltage pulse on the gate (by

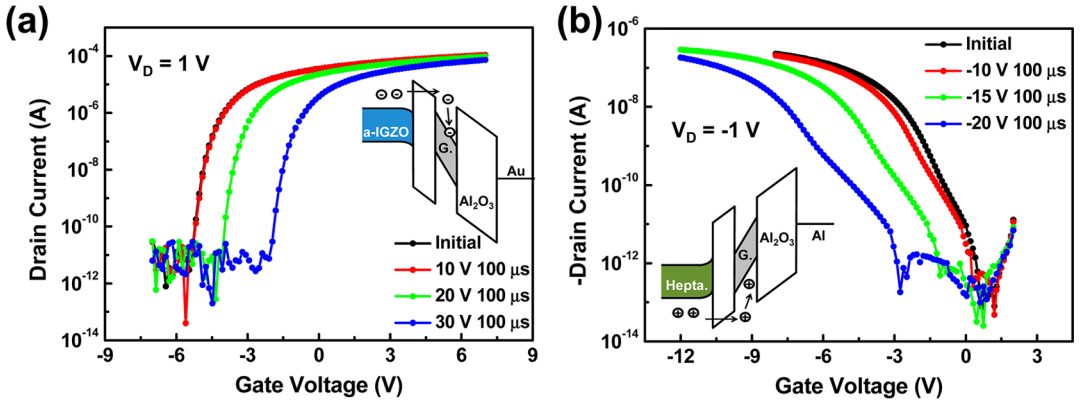

Figure 4. Transfer characteristics of the FET with guanine layer under the gate voltage pulse. Significant threshold voltage shifts are obtained (a) by top-gate top-contact a-IGZO FETs and (b) by bottom-gate top-contact heptzole FETs. Schematic band diagrams of our a-IGZO and heptazole FETs under Fowler–Nordheim tunneling are inset to the respective figures.

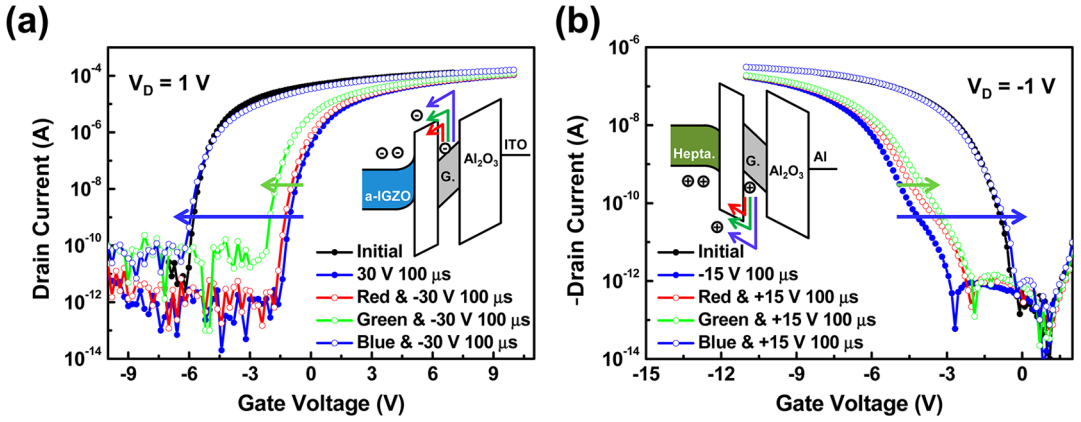

Figure 5. Transfer characteristics of the FETs under the negative voltage pulse and energetic photons (red, green, and blue). Full de-trapping of charges from the guanine layer is optimized with blue photons for (a) a-IGZO and (b) heptazole FETs, and its mechanism by photo illumination is shown as schematic energy band diagram as inset.

Fowler–Nordheim tunneling mechanism), resulting in ΔV_{th} toward a positive direction of transfer curve according to a simple device physics and electrostatics (we name this state as Program).[36−38] The threshold voltage shift by charges trapped in guanine layer can be expressed by following equations[39]

$$V_{th} = V_{FB} + \psi_s + \frac{Q_G}{C_{OX}} - \frac{Q_{guanine}X_{og}}{C_{OX}X_{OX}} \quad (1)$$

$$\Delta V_{th} = -\frac{Q_{guanine}X_{og}}{C_{OX}X_{OX}} \quad (2)$$

where V_{FB} is the flat-band voltage, ψ_s is the potential due to band bending of the channel semiconductor, Q_s is the charge per unit area associated with dielectric band bending as induced by gate bias, $Q_{guanine}$ is the injected charge (per unit area) in the guanine layer, C_{OX} is the total dielectric capacitance per unit area, X_{OX} is the total thickness of gate dielectric, and X_{og} is the thickness between gate and guanine. The positive voltage pulse effects on the FET with the guanine layer are displayed in detail with the transfer curves of Figure 4a, where ΔV_{th} effects by pulse voltage variation are observed (ΔV_{th} must be always positive according to eq 2 as electrons are trapped). According to Figure 4a, 10 V pulse does not make any ΔV_{th}, whereas small ΔV_{th} is achieved by 20 V pulse. A considerable ΔV_{th} of more than 3 V was obtained from 30 V pulse with 100 μs. Fowler–Nordheim tunneling easily explains such effects as shown with the inset band diagram of our FET device in Figure 4a. Under the high electric (E)-field with 30 V, the Al_2O_3 tunneling layer is seriously bent to make a triangular shape of barrier wall, so that the accumulated electrons at the IGZO channel easily tunnel through the thin barrier and then begin to occupy the LUMO state of guanine (because the HOMO state is always occupied by electrons in general). It is remarkable that without thermal or photo energy-induced aid, the guanine-trapped electrons cannot easily escape but should stay there infinitely due to the barrier height. Negative bias of −30 V could not release the trapped electrons because, in this case, a-IGZO layer is electrically depleted by the negative pulse voltage and takes quite a voltage drop in its thickness (see Figure S5 in the Supporting Information shows more details of −30 V pulse-driven results). Likewise, in the thin-film based FETs, Program state (by charge trapping) is only visible but Erase state (by escaping/de-trapping) is rare to see in report.[16,40−43] Besides the application to inorganic a-IGZO FET, we also applied same mechanism to p-channel organic FET with small molecule, 8,16-dihydrobenzo[a]benzo[6,7]indolo[2,3-h]carbazole (heptazole: $C_{26}H_{16}N_2$) which appeared more photostable than widely used organic small molecule, pentacene.[44] Since ALD process would seriously damage the heptazole organic channel layer, our organic FET was fabricated with bottom gate structure as shown in Figure S6 in the Supporting Information.

dx.doi.org/10.1021/am405998d | ACS Appl. Mater. Interfaces 2014, 6, 4965−4973

With sufficient gate voltage to make thin Al_2O_3 barrier thickness as triangular shape, hole charges can be injected from heptazole active to guanine trapping layer (inset in Figure 4b). A considerable ΔV_{th} was achieved by more than −15 V pulse in this case, which is relatively smaller than that in the former case of a-IGZO FET; it is mainly because organic heptazole has smaller hole barrier to ALD Al_2O_3 than the electron barrier of a-IGZO to the same dielectric (detail estimation is shown in Figure S7 and Table S2 in the Supporting Information).

Practical way of erasing (de-trapping the electrons trapped in the DNA-base well) is probably by using energetic photons; in fact our inorganic and organic FET devices underwent such photoinduced erasing as shown in panels a and b in Figure 5. According to photo-transfer curve and the inset schematic of Figure 5a, our guanine-embedded FETs with transparent indium−tin-oxide (ITO) gate are illuminated by energetic photons simultaneously under the condition of −30 V 100 μs pulse, and only blue photons of 440 nm appear very effective for de-trapping while the other spectra (red and green) with lower energy than that of blue result in only a little effect. (Of course, a −30 V pulse without any illumination never works as evidenced by Figure S4a, b in the Supporting Information). In view of the electron affinity (2.48 eV) of organic guanine layer (Figure 1a), it is certain that more chances would be provided to trapped electrons by the photons whose energy is even higher than 2.48 eV. Along with the a-IGZO case, the hepazole organic FETs also show similar behavior with energetic photons. As shown in Figure 5b, the injected hole charges can only be fully recovered by blue photons of 440 nm, whereas low energy photons (red and green) do hardly induce any significant detrapping probably due to the barrier between guanine HOMO and Al_2O_3 valence band maximum. In the present study, the programming by Fowler−Nordheim tunneling and erasing by blue energetic photon were the most optimal ways to demonstrate any feasibility of the nonvolatile charge injection/photo memory application.

D. Boolean Logic Gate Application Using Guanine Trapping Layer. On the basis of aforementioned trapping effects by guanine layer, we here extend such program effects to a logic inverter and Boolean logic applications using inorganic a-IGZO FETs.[45,46] Trapped and staying in the guanine layer, the injected electron charges induce the positive threshold voltage shift as discussed in 2.2. Programmed (30 V 100 μs pulse) and unprogrammed FETs (Initial) with their respective transfer curves (Figure 4a) would now play as driver and load in an inverter (NOT gate logic) if they are coupled each other as shown in the optical microscopy of Figure 1b. Because the V_{th} of our programmed FET becomes close to zero volts after the pulse in Figure 4a, we could obtain a high-to-low transition voltage of our inverter at a positive voltage (as 0−2 V) as seen in the voltage transfer characteristic (VTC) curves of Figure 6a. Interestingly, the program state of our driver FET with guanine trap layer was so fixed without any fluctuation that our inverter showed only a little change (< 0.3 V) in its VTC characteristics even after 10 days pass in ambient. Moreover, according to the inset graph of V_{out} versus time in Figure 6a, V_{out} of our inverter almost maintains its initial value under a critical bias stress condition: 10000 s at V_{DD} = 10 V and V_{in} of 2 V (which is the transition voltage). These results mean that the trapped charges in guanine stably stay within the 20 nm thin DNA-base guanine layer. The inset circuit of Figure 6b distinguishes programmed (driver) and unprogrammed (load) FETs with the thick black bar in FET, whereas the red line in both FETs indicates the embedded DNA-base layer. Voltage gain (= $-dV_{out}/dV_{in}$) appears not that high, to be 4.2 at a supply voltage (V_{DD}) of 10 V, because the V_{th} of programmed FET by 30 V pulse yet stays in a negative voltage region. However, the value would be optimized by reducing the blocking Al_2O_3 layer thickness, and our inverter still seems very effective, dynamically playing as a logic device. Under 10 V V_{DD}, our inverter shows less than 50 ms switching time according to its 2 and 10 Hz operations in Figure 6c. Because such programming was possible for every FET cell with guanine layer, NAND and NOR gate logics were simply demonstrated with 1 unprogrammed and 2 programmed FETs as respectively seen in panels a and b in Figure 7. Because NAND and NOR logic gates need two driver transistors, one additional programmed transistor was achieved by the same condition of 30 V 100 μs gate pulse. Two programmed FETs were then connected in series for NAND logic and in parallel for NOR logic. As a result, two static VTC curves were obtained by scanning $V_{in,1}$ from −5 V to 10 V under two fixed $V_{in,2}$ voltages: −5 V and 10 V (here, we used the two input voltages of −5 V and 10 V as logic signal 0 and 1, respectively). Logic truth tables for NAND and NOR Boolean logics are

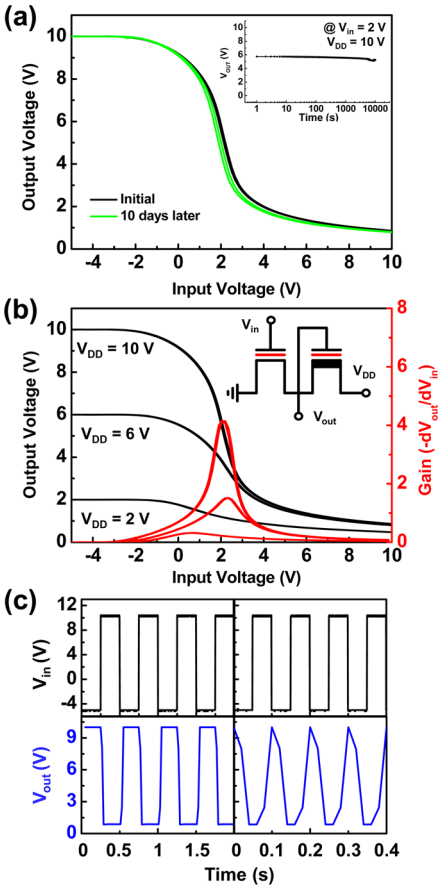

Figure 6. (a) Inverter retention properties are shown by VTC curve after 10 days in ambient and also by stable output voltage value under a critical bias stress V_{DD} = 10 V and V_{in} = 2 V (inset). (b) Static voltage transfer characteristics (VTC) curve of our inverter logic circuit under several V_{DD} conditions (V_{DD} = 10 V, 6 V, 2 V). The thick black bar indicates the channel of Un-programmed FET while the red line indicates the embedded guanine layer in the inset circuit. (c) Dynamic inverter behavior under V_{DD} = 10 V, 2 Hz (left column) and 10 Hz (right) operation.

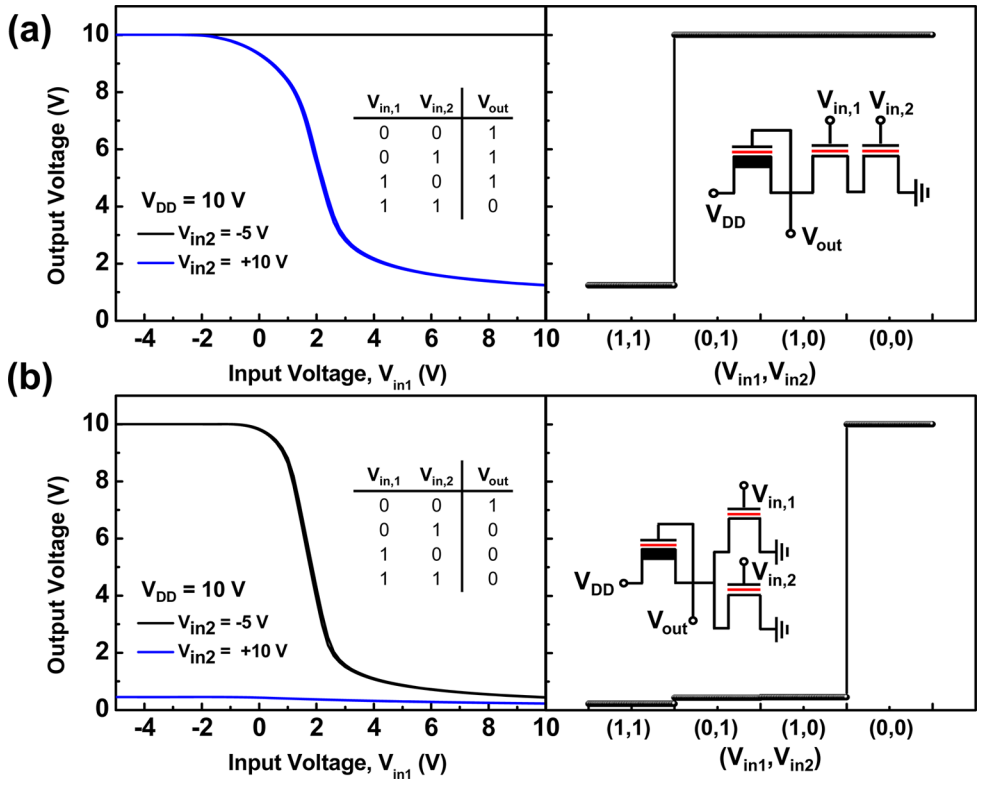

Figure 7. Static and dynamic VTC behavior of (a) NAND and (b) NOR logic gates using DNA-base embedded dielectric. One Un-programmed and two Programmed FETs were connected for NAND and NOR logic functions as shown in the inset circuits of (a) and (b), respectively. Above figures for NAND and NOR functions, we suggested logic (1,0) as (10 V, −5 V) to get clear logic signals. Truth tables of both Boolean logics are summarized as insets to the respective plots.

summarized in the inset table of Figure 7, and its operations are well-demonstrated.

SUMMARY

In summary, we have performed unprecedented applications of DNA-base guanine layer for modern FET devices. Embedded with the layer in dielectric oxide during ALD process, our IGZO FET becomes more electrically stable since the guanine layer getters H atoms during ALD-oxide growth process. Moreover, the embedded guanine layer plays as a charge trapping layer for not only channel-injected electrons of a-IGZO, but also injected holes of heptazole. The photon-assisted erasing function is also accomplished when the injected charges are recovered to both the inorganic and organic channels by the aid of blue photon energy under proper voltage pulse. Finally, basic Boolean logics such as NOT, NAND and NOR are stably demonstrated using the programmed and unprogrammed FETs. We conclude that our DNA-base guanine layer is novel and promising enough to be used as an important component for electrically stable FETs, photo-memory and FET-based logic.

ASSOCIATED CONTENT

Supporting Information

XRD and AFM data of guanine film, absorption spectra of DNA-base layers; transfer characteristics of a-IGZO FETs under multiple gate voltage sweep; linear mobility of the a-IGZO FETs after PBS test; negative voltage pulse-driven transfer characteristics of the a-IGZO FET; positive voltage pulse driven transfer characteristics of the heptazole FET; device structure of organic heptazole FETs; schematic band diagrams of our organic heptazole and inorganic a-IGZO FETs with vacuum-level (E_{vac}) alignment; reported literature values of the electron binding energy (B.E.) of oxygen 1s (O 1s) and aluminum 2p (Al 2p) orbitals for Al_2O_3, $Al(OH)_3$, AlO(OH); reported literature values of electron affinity, band gap, ionization energy, and calculated barrier height for Al_2O_3, guanine, heptzole, a-IGZO. This material is available free of charge via the Internet at http://pubs.acs.org.

AUTHOR INFORMATION

Corresponding Author

*E-mail semicon@yonsei.ac.kr. Tel: +82-2-2123-2842. Fax: +82-2-392-1592.

Notes

The authors declare no competing financial interest.

ACKNOWLEDGMENTS

This research was supported by Nano. Material Technology Development Program (Grant no. 2012M3A7B4049801), NRL program (Grant 2009-0079462) and BK 21 plus through the National Research Foundation of Korea (NRF) funded by the Ministry of Education, Science and Technology. Authors also give thanks to H. J. Choi, J. H. Kim, K. J. Choi for valuable discussion.

REFERENCES

(1) Braun, E.; Eichen, Y.; Sivan, U.; Ben-Yoseph, G. DNA-Templated Assembly and Electrode Attachment of a Conducting Silver Wire. *Nature* **1998**, *391*, 775−778.

(2) Keren, K.; Berman, R. S.; Buchstab, E.; Sivan, U.; Braun, E. DNA-Templated Carbon Nanotube Field-Effect Transistor. *Science* **2003**, *302*, 1380−1382.
(3) Maruccio, G.; Visconti, P.; Arima, V.; D'Amico, S.; Biasco, A.; D'Amone, E.; Cingolani, R.; Rinaldi, R.; Masiero, S.; Giorgi, T. Field Effect Transistor Based on a Modified DNA Base. *Nano Lett.* **2003**, *3*, 479−483.
(4) Seeman, N. C. DNA in a Material World. *Nature* **2003**, *421*, 427−431.
(5) Yan, H.; Park, S. H.; Finkelstein, G.; Reif, J. H.; LaBean, T. H. DNA-Templated Self-Assembly of Protein Arrays and Highly Conductive Nanowires. *Science* **2003**, *301*, 1882−1884.
(6) Hagen, J. A.; Li, W.; Steckl, A.; Grote, J. Enhanced Emission Efficiency in Organic Light-Emitting Diodes Using Deoxyribonucleic Acid Complex as an Electron Blocking Layer. *Appl. Phys. Lett.* **2006**, *88*, 171109.
(7) Steckl, A. J. DNA − a New Material for Photonics? *Nat. Photonics* **2007**, *1*, 3.
(8) Kim, Y. S.; Jung, K. H.; Lee, U. R.; Kim, K. H.; Hoang, M. H.; Jin, J.-I.; Choi, D. H. High-Mobility Bio-Organic Field Effect Transistors With Photoreactive DNAs as Gate Insulators. *Appl. Phys. Lett.* **2010**, *96*, 103307.
(9) Singh, B.; Sariciftci, N. S.; Grote, J. G.; Hopkins, F. K. Bio-Organic-Semiconductor-Field-Effect-Transistor Based on Deoxyribonucleic Acid Gate Dielectric. *J. Appl. Phys.* **2006**, *100*, 024514.
(10) Stadler, P.; Oppelt, K.; Singh, T. B.; Grote, J. G.; Schwödiauer, R.; Bauer, S.; Piglmayer-Brezina, H.; Bäuerle, D.; Sariciftci, N. S. Organic Field-Effect Transistors and Memory Elements Using Deoxyribonucleic Acid (DNA) Gate Dielectric. *Org. Electron.* **2007**, *8*, 648−654.
(11) Yukimoto, T.; Uemura, S.; Kamata, T.; Nakamura, K.; Kobayashi, N. Non-Volatile Transistor Memory Fabricated Using DNA and Eliminating Influence of Mobile Ions on Electric Properties. *J. Mater. Chem.* **2011**, *21*, 15575−15579.
(12) Yumusak, C.; Singh, T. B.; Sariciftci, N.; Grote, J. Bio-Organic Field Effect Transistors Based on Crosslinked Deoxyribonucleic Acid (DNA) Gate Dielectric. *Appl. Phys. Lett.* **2009**, *95*, 263304.
(13) Irimia-Vladu, M.; Głowacki, E. D.; Voss, G.; Bauer, S.; Sariciftci, N. S. Green and Biodegradable Electronics. *Mater. Today* **2012**, *15*, 340−346.
(14) Irimia-Vladu, M.; Sariciftci, N. S.; Bauer, S. Exotic Materials for Bio-Organic Electronics. *J. Mater. Chem.* **2011**, *21*, 1350−1361.
(15) Irimia-Vladu, M.; Troshin, P. A.; Reisinger, M.; Shmygleva, L.; Kanbur, Y.; Schwabegger, G.; Bodea, M.; Schwödiauer, R.; Mumyatov, A.; Fergus, J. W.; Razumov, V. F.; Sitter, H.; Sariciftci, N. S.; Bauer, S. Biocompatible and Biodegradable Materials for Organic Field-Effect Transistors. *Adv. Funct. Mater.* **2010**, *20*, 4069−4076.
(16) Leong, W.L.; Mathews, N.; Tan, B.; Vaidyanathan, S.; Dotz, F.; Mhaisalkar, S. Towards Printable Organic Thin Film Transistor Based Flash Memory Devices. *J. Mater. Chem.* **2011**, *21*, 5203−5214.
(17) Sekitani, T.; Yokota, T.; Zschieschang, U.; Klauk, H.; Bauer, S.; Takeuchi, K.; Takamiya, M.; Sakurai, T.; Someya, T. Organic Nonvolatile Memory Transistors for Flexible Sensor Arrays. *Science* **2009**, *326*, 1516−1519.
(18) Kim, S.-J.; Lee, J.-S. Flexible Organic Transistor Memory Devices. *Nano Lett.* **2010**, *10*, 2884−2890.
(19) Baeg, K.-J.; Noh, Y.-Y.; Ghim, J.; Lim, B.; Kim, D.-Y. Polarity Effects of Polymer Gate Electrets on Non-Volatile Organic Field-Effect Transistor Memory. *Adv. Funct. Mater.* **2008**, *18*, 3678−3685.
(20) Lee, Y.; Lee, H.; Park, S.; Yi, Y. Energy Level Alignment at the Interfaces Between Typical Electrodes and Nucleobases: Al/Adenine/Indium-Tin-Oxide and Al/Thymine/Indium-Tin-Oxide. *Appl. Phys. Lett.* **2012**, *101*, 233305.
(21) Maia, F.; Freire, V.; Caetano, E.; Azevedo, D.; Sales, F.; Albuquerque, E. Anhydrous Crystals of DNA Bases Are Wide Gap Semiconductors. *J. Chem. Phys.* **2011**, *134*, 175101.
(22) Šponer, J.; Leszczynski, J.; Hobza, P. Nature of Nucleic Acid-Base Stacking: Nonempirical ab Initio and Empirical Potential Characterization of 10 Stacked Base Dimers. Comparison of Stacked and H-Bonded Base Pairs. *J. Phys. Chem.* **1996**, *100*, 5590−5596.
(23) Hosono, H. Ionic Amorphous Oxide Semiconductors: Material Design, Carrier Transport, and Device Application. *J. Non-Cryst. Solids* **2006**, *352*, 851−858.
(24) Nomura, K.; Ohta, H.; Takagi, A.; Kamiya, T.; Hirano, M.; Hosono, H. Room-Temperature Fabrication of Transparent Flexible Thin-Film Transistors Using Amorphous Oxide Semiconductors. *Nature* **2004**, *432*, 488−492.
(25) Biesinger, M.C. X-ray Photoelectron Spectroscopy Reference Pages. http://www.xpsfitting.com/search/label/Aluminum (accessed Feb 7, 2014).
(26) Naumkin, A. V.; Kraut-Vass, A.; Gaarenstroom, S. W.; Powell, C. J. NIST X-ray Photoelectron Spectroscopy Database. http://srdata.nist.gov/xps/ (accessed Feb 7, 2014).
(27) George, S. M. Atomic Layer Deposition: An Overview. *Chem. Rev.* **2010**, *110*, 111−131.
(28) Groner, M.; Fabreguette, F.; Elam, J.; George, S. Low-Temperature Al_2O_3 Atomic Layer Deposition. *Chem. Mater.* **2004**, *16*, 639−645.
(29) Verdolino, V.; Cammi, R.; Munk, B.H.; Schlegel, H.B. Calculation of pKa Values of Nucleobases and the Guanine Oxidation Products Guanidinohydantoin and Spiroiminodihydantoin using Density Functional Theory and a Polarizable Continuum Model. *J. Phys. Chem. B* **2008**, *112*, 16860−16873.
(30) Jang, Y.H.; Goddard, W.A., III; Noyes, K.T.; Sowers, L.C.; Hwang, S.; Chung, D.S. pKa Values of Guanine in Water: Density Functional Theory Calculations Combined with Poisson-Boltzmann Continuum-Solvation Model. *J. Phys. Chem. B* **2003**, *107*, 344−357.
(31) Dingemans, G.; Beyer, W.; Sanden, M.; Kessels, W. Hydrogen Induced Passivation of Si Interfaces by Al_2O_3 Films and SiO_2/Al_2O_3 Stacks. *Appl. Phys. Lett.* **2010**, *97*, 152106.
(32) Choi, S.-H.; Jang, J.-H.; Kim, J.-J.; Han, M.-K. Low-Temperature Organic (CYTOP) Passivation for Improvement of Electric Characteristics and Reliability in IGZO TFTs. *IEEE Electron Device Lett.* **2012**, *33*, 381−383.
(33) Kim, H. J.; Park, S. Y.; Jung, H. Y.; Son, B. G.; Lee, C.-K.; Lee, C.-K.; Jeong, J. H.; Mo, Y.-G.; Son, K. S.; Ryu, M. K. Role of Incorporated Hydrogen on Performance and Photo-Bias Instability of Indium Gallium Zinc Oxide Thin Film Transistors. *J. Phys. D: Appl. Phys.* **2013**, *46*, 055104.
(34) Lee, J.; Park, J.-S.; Pyo, Y. S.; Lee, D. B.; Kim, E. H.; Stryakhilev, D.; Kim, T. W.; Jin, D. U.; Mo, Y.-G. The Influence of the Gate Dielectrics on Threshold Voltage Instability in Amorphous Indium-Gallium-Zinc Oxide Thin Film Transistors. *Appl. Phys. Lett.* **2009**, *95*, 123502.
(35) Sung, S.-Y.; Choi, J. H.; Han, U. B.; Lee, K. C.; Lee, J.-H.; Kim, J.-J.; Lim, W.; Pearton, S.; Norton, D.; Heo, Y.-W. Effects of Ambient Atmosphere on the Transfer Characteristics and Gate-Bias Stress Stability of Amorphous Indium-Gallium-Zinc Oxide Thin-Film Transistors. *Appl. Phys. Lett.* **2010**, *96*, 102107.
(36) Lenzlinger, M.; Snow, E. Fowler Nordheim Tunneling into Thermally Grown SiO_2. *J. Appl. Phys.* **1969**, *40*, 278−283.
(37) Lin, H.; Ye, P.; Wilk, G. Leakage Current and Breakdown Electric-Field Studies on Ultrathin Atomic-Layer Deposited Al_2O_3 on GaAs. *Appl. Phys. Lett.* **2005**, *87*, 182904.
(38) Sze, S.M.; Kwok, K. Ng. In *Physics of Semiconductor Device*; Wiley-Interscience: Hoboken, NJ, 2007; Chapter 6, pp 352−360.
(39) Muller, R. S.; Kamins, T. I.; Chan, M. In *Device Electronics for Integrated Circuits*; Wiley: Hoboken, NJ, 2003; Chapter 10, pp 507−513.
(40) Cha, S. H.; Park, A.; Lee, K. H.; Im, S.; Lee, B. H.; Sung, M. M. Pentacene Thin-Film on Organic/Inorganic Nanohybrid Dielectrics for ZnO Charge Injection Memory Transistor. *Org. Electron.* **2010**, *11*, 159−163.
(41) Suresh, A.; Novak, S.; Wellenius, P.; Misra, V.; Muth, J. F. Transparent Indium Gallium Zinc Oxide Transistor Based Floating Gate Memory with Platinum Nanoparticles in the Gate Dielectric. *Appl. Phys. Lett.* **2009**, *94*, 123501.

(42) Yin, H.; Kim, S.; Kim, C. J.; Song, I.; Park, J.; Kim, S.; Park, Y. Fully Transparent Nonvolatile Memory Employing Amorphous Oxides as Charge Trap and Transistor's Channel Layer. *Appl. Phys. Lett.* **2008**, *93*, 172109.
(43) Yin, H.; Kim, S.; Lim, H.; Min, Y.; Kim, C. J.; Song, I.; Park, J.; Kim, S.; Tikhonovsky, A.; Hyun, J.; Park, Y. Program/Erase Characteristics of Amorphous Gallium Indium Zinc Oxide Nonvolatile Memory. *IEEE Trans. Electron Devices* **2008**, *55*, 2071−2077.
(44) Park, J. H.; Lee, H. S.; Park, S.; Min, S. W.; Yi, Y.; Cho, C. G.; Han, J.; Kim, T. W.; Im, S. *Adv. Funct. Mater.* DOI: 10.1002/adfm.201301783.
(45) Cha, S. H.; Oh, M. S.; Lee, K. H.; Choi, J.-M.; Lee, B. H.; Sung, M. M.; Im, S. ZnO-Based Low-Voltage Inverter With Quantum-Well-Structured Nanohybrid Dielectric. *IEEE Electron Device Lett.* **2008**, *29*, 1145−1147.
(46) Lee, Y. T.; Raza, S. R. A.; Jeon, P. J.; Ha, R.; Choi, H.-J.; Im, S. Long Single ZnO Nanowire for Logic and Memory Circuits: NOT, NAND, NOR Gate, and SRAM. *Nanoscale* **2013**, *5*, 4181−4185.